Phonon dispersion curves of stable and metastable BC$_3$ honeycomb epitaxial sheets and their chemical bonding: Experiment and theory

H. Yanagisawa,[1,2,*] T. Tanaka,[1,2] Y. Ishida,[1,2] E. Rokuta,[1,2] S. Otani,[3] and C. Oshima[1,2]

[1]*Department of Applied Physics, Waseda University, 3-4-1 Okubo, Shinjuku-ku Tokyo 169-8555, Japan*

[2]*Kagami Memorial Laboratory for Material Science and Technology, Waseda University, 2-8-26, Nishiwaseda, Shinjuku-ku, Tokyo 169-0051, Japan*

[3]*National Institute for Material Science, 1-1, Namiki, Tsukuba-shi, Ibaraki 305-0044, Japan*

We have investigated experimentally and theoretically the phonon-dispersion curves along the $\bar{\Gamma}$-$\bar{M}$ axis in two-dimensional surface Brillouin zones of the stable and metastable BC$_3$ honeycomb sheets with different lattice constants. Most of the observed curves agreed with the theoretical ones calculated on the basis of the *ab initio* theory. There exists a common relationship between the nearest-neighbor stretching force constants and bond lengths of two-dimensional honeycomb structures in various compounds of boron, carbon, and nitrogen; the two-dimensional bonds are discriminated clearly from the one- and three-dimensional bonds. We detected a librational mode of carbon hexagons in BC$_3$; a peculiar mode for a large unit cell of honeycomb sheets such as the 2×2 structure of monolayer graphite and BC$_3$. The restoring force related with the bond bending is insensitive to the change in the B-C bond length.

PACS number(s): 68.35.Ja, 63.20.Dj, 68.35.Dv, 68.55.Jk

I. INTRODUCTION

New groups of graphitic materials constituted by boron, carbon, and nitrogen have stimulated fundamental explorations in material science because they exhibit a very wide variety of chemical and physical properties depending on their bonding manners and their chemical compositions. Some compounds such as graphite, fullerene, nanotube, and *hexagonal* boron nitride (*h*-BN) were exhaustively investigated both experimentally and theoretically in various research fields such as the development of electronic devices and electrodes of batteries, and fundamental physics.[1–4] The other compounds with boron-carbon honeycomb structures such as BC and BC$_3$ were investigated theoretically in relation to their high superconducting transition temperatures (T_c) of CuBC, LiBC, and Mg$_2$BC$_3$,[5–8] being isomorphic of MgB$_2$ (T_c=39 K).[9] Since no macroscopic single crystals of these materials were available so far,[10,11] however, little is known experimentally.

As we reported elsewhere,[12–14] we grew two kinds of uniform BC$_3$ honeycomb sheets with different lattice constants with excellent crystalline quality over macroscopic surface areas of NbB$_2$(0001), which were investigated by low-energy electron diffraction (LEED), x-ray photoemission spectroscopy (XPS), Auger electron spectroscopy (AES), ultraviolet photoemission spectroscopy (UPS), and scanning tunneling microscopy (STM). Hereafter, we call them the stable BC$_3$ (*s*-BC$_3$) and metastable BC$_3$ (*m*-BC$_3$). The *m*-BC$_3$ changes irreversibly to the *s*-BC$_3$ by heating, and the *m*-BC$_3$ can be prepared only by carbon substitution in boron honeycomb sheets. All the observed data on the chemical composition, the lattice constant, the LEED intensity distribution, and the electronic band structure indicated clearly that both the BC$_3$ honeycomb sheets were uniformly grown in an epitaxial way to the substrate lattice. Those are macroscopic uniform films of the single-crystal BC$_3$ sheets.

Previously, we have reported the phonon-dispersion curves of the *s*-BC$_3$ honeycomb sheets along the $\bar{\Gamma}$-$\bar{M}$ axis

and compared them with the theoretical curves calculated on the basis of the *ab initio* theory. In this paper, we report the detailed phonon structures in both the *s*- and *m*-BC$_3$ investigated experimentally and theoretically. The measured and calculated phonon-dispersion curves were in good agreement with each other for both the sheets. We discussed the common relationship between stretching force constants and their bond lengths of nearest-neighbor bonds constituted by boron, carbon, and nitrogen. Characteristic features of the 2×2 structure of monolayer graphite such as a rotational-displacement mode of a whole carbon hexagon were pointed out in the phonons of the sheets; the similar vibrational energies of the mode were observed in the two sheets.

II. METHODOLOGY

A. Experiment

The experiments were carried out in an ultrahigh vacuum (UHV) chamber (ground pressure $<2 \times 10^{-8}$ Pa) equipped with a cylindrical mirror analyzer for Auger-electron spectroscopy (AES), a low-energy electron diffraction (LEED) optics, and a high-resolution electron-energy-loss spectrometer (HREELS: SPECS Delta0.5) for measurement of phonon-dispersion curves.

Both the *s*- and *m*-BC$_3$ sheets were grown in an epitaxial way to the NbB$_2$(0001) substrate lattice, as we reported in our other papers.[12,13] To grow the BC$_3$ honeycomb sheets, we utilized the surface segregation of the carbon impurities in NbB$_2$. The single crystal of NbB$_2$ was grown by use of the floating zone method,[15] and the main impurities were 30 ppm of carbon. By heating up to temperature of 1100 °C, the *m*-BC$_3$ honeycomb sheets were grown in a commensurate manner on the NbB$_2$(0001) surface; LEED and STM showed the $\sqrt{3} \times \sqrt{3}$ structure. With successive heatings at 1300 °C, the *m*-BC$_3$ sheet changed irreversibly to the incommensurate *s*-BC$_3$ sheet. The lattice constant of the

s-BC$_3$ was shorter than that of the *m*-BC$_3$ by 0.02 nm. In the angle-resolved x-ray photoemission spectroscopy (ARXPS) and AES spectra of the two BC$_3$ sheets, no difference in the chemical concentration was detected within the experimental accuracy; the stoichiometric ratio of boron to carbon was around 1 to 3.[12,14] The LEED patterns showed clear diffraction spots indicative of either the *s*- or *m*-BC$_3$ sheets, each of which was clearly distinguishable from the other.

The HREEL spectra were measured along the $\bar{\Gamma}$-$\bar{M}$ axis in two-dimensional surface Brillouin zones (SBZs). The incident angle θ_i was fixed at 75 deg and the scattering angle θ_s was varied to change the wave vector of the excited phonons parallel to the sheet surface. The incident energies E_0 were 18.1 and 24.7 eV for the *s*-BC$_3$ and 24.7 eV for the *m*-BC$_3$. The energy resolution was 2–3 meV at the sample current of about 1×10^{-10} A. Little contamination was detected on the surface after a few days elapsed in a (ultra-high vacuum) UHV, because the BC$_3$ sheets are chemically inert similar to the graphite sheets. Typical measuring time for one spectrum was about 1 h under specular conditions and 4–5 h under off-specular conditions.

B. Theoretical analysis

The theoretical phonon-dispersion curves were obtained on the basis of *ab initio* calculations (DACAPO package[16]). The ultrasoft pseudopotentials[17] are employed for both boron and carbon atoms. Plane-wave functions with a cutoff energy at 36.7 Ry were used as the basis set and the generalized gradient approximation (GGA)[18] for the exchange-correlation potential. Brillouin zone *k*-points sampling grids are $16 \times 4 \times 1$ according to the Monkhorst-Pack scheme.[19] The fundamental procedure to calculate phonon-dispersion curves was the same as that proposed by Kunc *et al.*[20] A rectangular-shaped supercell containing 32 atoms was used, and each layer was separated by 12 Å vacuum in the calculations of both the BC$_3$. The dynamical-matrix elements were evaluated from the Hellmann-Feynman forces generated by a slight displacement of the linearly chained atoms. The displacement length was 0.0005 nm in all the calculations. Essentially, our calculation was the same with Dubay *et al.*,[21] only the difference lies in the definition of the supercell, which is used to extract the Hellmann-Feyman forces. The equivalent phonon-dispersion curves of the graphene sheet were obtained as Dubay *et al.* did. In previous papers, we confirmed the obtained curves were in good agreement with the measured graphite data.[13,22] Thus, our theoretical calculations ensure reliability in the investigation of the isostructural BC$_3$ honeycomb sheets.

In the calculation of the lattice dynamics of the two BC$_3$ sheets, we employed the atomic structure model depicted schematically in Fig. 1. The precise atomic structure of the *s*-BC$_3$ sheet was determined theoretically to yield the highest cohesive energy among possible structures with the same chemical composition.[23] The lattice constant and atomic positions in a unit cell were optimized by iterative loops of the calculations with the hexagonal symmetry maintained, and the results were almost the same as that of the reported ones;[24] the nearest-neighbor C-C and B-C bond lengths, l_{C-C}
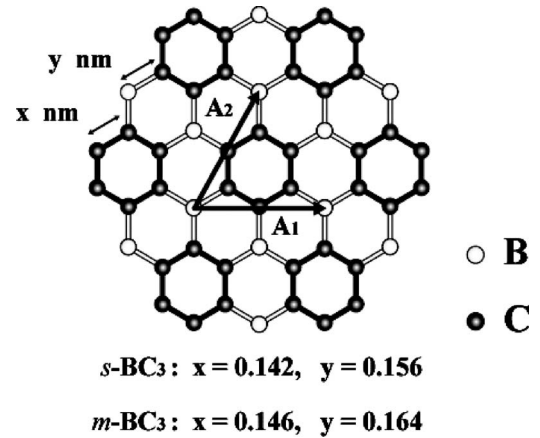
FIG. 1. A schematic representation of the *s*- and *m*-BC$_3$ atomic structures optimized by the *ab initio* calculations. White circles and black circles denote B and C atoms, respectively. The vectors, $\mathbf{A}_1$ and $\mathbf{A}_2$, are primitive translational vectors of BC$_3$.

and l_{B-C}, were 0.142 and 0.156 nm, respectively.[25] The half of the calculated lattice constant, 0.26 nm, was in good agreement with the one yielded by LEED, 0.26 ± 0.002 nm.[12] In the determination of the atomic structure of the *m*-BC$_3$ sheet, we assumed the atomic arrangement depicted in Fig. 1. The lattice constant of the *m*-BC$_3$ sheet was fixed to 0.537 nm, which was determined by the LEED pattern. Only the atomic positions in a unit cell were adjusted to minimize the total-energy; the optimum values were l_{C-C}=0.146 nm and l_{B-C}=0.164 nm for the *m*-BC$_3$ sheet.

The cohesive energies with respect to isolated atoms have been evaluated within the GGA. The cohesive energies of one formula unit of the two BC$_3$ sheets were very close to each other; they are −32.48 eV for the *s*-BC$_3$ and −32.14 eV for the *m*-BC$_3$, which corresponds to the average cohesion per atom of −8.12 and −8.04 eV. They are slightly higher than the calculated graphite value of −8.64 eV per atom because of the existence of the B-C bonds.

To understand the nature of the local bonding in the BC$_3$ sheets, we calculated interatomic stretching force constants (FCs) of nearest-neighbor C-C and B-C bonds. By using the 3×3 unit cell of a BC$_3$ sheet as a supercell, the stretching FCs of C-C (B-C) bonds were calculated from the Hellmann-Feynman forces generated by displacing one carbon (boron) atom along its nearest-neighbor C-C (B-C) bond, while all other atoms are kept at their equilibrium positions.

III. RESULTS AND DISCUSSION

A. Phonon-dispersion curves of the *s*- and *m*-BC$_3$ sheets

In Figs. 2 and 3, we show the HREEL spectra of the *s*- and *m*-BC$_3$/NbB$_2$(0001) measured along the $\bar{\Gamma}$-$\bar{M}$ axis in two-dimensional SBZs depicted by solid lines in Fig. 4. The incident energy E_0 was 24.7 eV in each spectrum. The observed peaks in the specular spectra (q=0) were mainly generated by dipole electric fields excited by vibrations with out-of-plane polarization, while those in the off-specular spectra ($q \neq 0$) were mostly generated by microscopic atomic
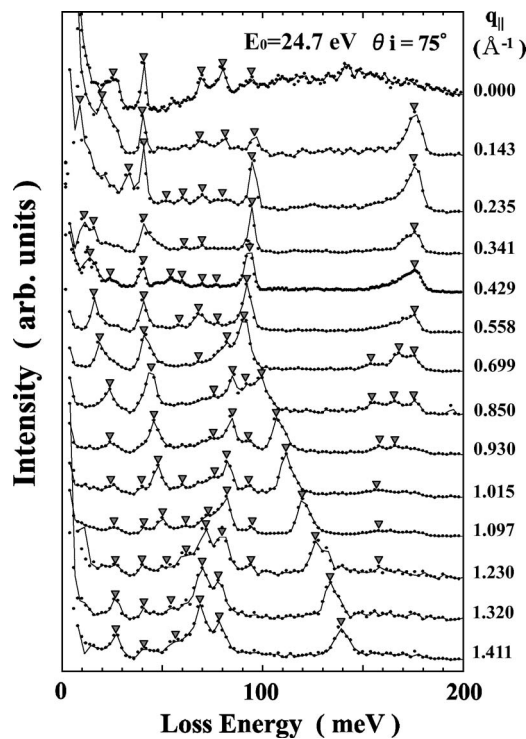
FIG. 2. The HREEL spectra of the monolayer s-BC$_3$ film on NbB$_2$(0001) as a function of wave vectors along the $\bar{\Gamma}$-$\bar{M}$ axis. The incident energy E_0 was 24.7 eV. The positions of loss peaks are denoted by triangles.
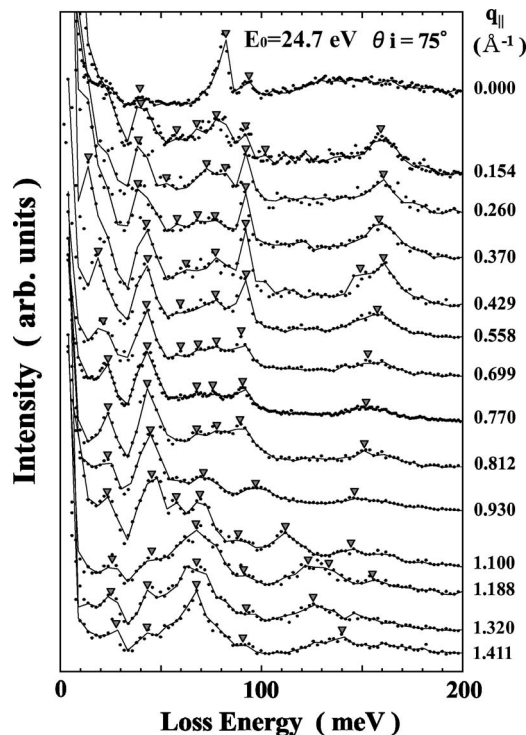
FIG. 3. The HREEL spectra of the monolayer m-BC$_3$ film on NbB$_2$(0001) as a function of wave vectors along the $\bar{\Gamma}$-$\bar{M}$ axis. The incident energy E_0 was 24.7 eV. The positions of loss peaks are denoted by triangles.
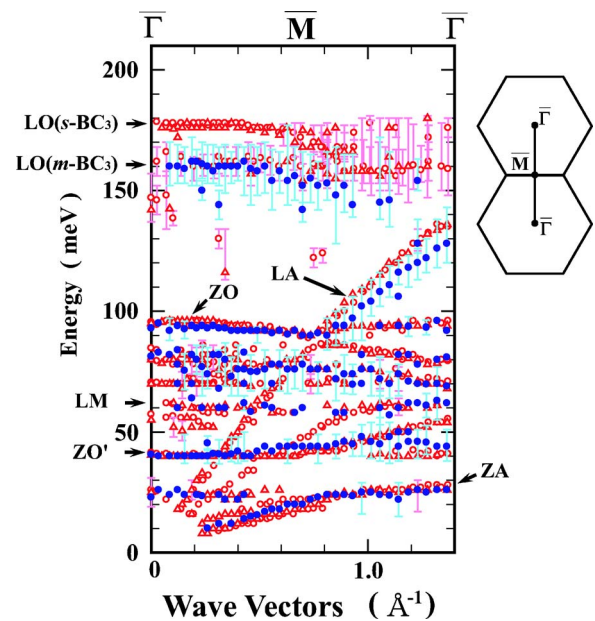
FIG. 4. (Color online) The observed dispersion curves along the $\bar{\Gamma}$-$\bar{M}$ axis of the s- and m-BC$_3$ sheets (red open circles and red open triangles for the s-BC$_3$, blue solid circle for the m-BC$_3$). Some characteristic branches are denoted by capital letters, see the text. Hexagonal zones framed by solid lines represent the SBZ of BC$_3$.

potential. As denoted by the triangles in Fig. 2, at least seven loss peaks were recognizable in isolation in the spectra; the number of peaks was larger than that of graphite,[26] which corresponds to the large unit cell of the s-BC$_3$ in comparison with graphite. All the peaks in the spectra of the m-BC$_3$ in Fig. 3 were broader and less recognizable as compared with the peaks of the s-BC$_3$, which suggests that the crystalline quality of the m-BC$_3$ sheet is worse than that of the s-BC$_3$.[27] The highest vibrational energies of the observed phonons were 180 and 160 meV for the s- and m-BC$_3$ sheets, respectively. They were above the maximum phonon energies of metal diborides, about 90 meV,[28,29] and below that of graphite, about 200 meV.[26]

By plotting the loss energies in the HREEL spectrum against the wave vector, we determined the dispersion curves of the two sheets as shown in Fig. 4. The experimental data points are represented by red open circles and red open triangles for the s-BC$_3$ for $E_0=18.1$ and 24.7 eV, respectively, and blue solid circles for the m-BC$_3$ for $E_0=24.7$ eV. The longitudinal acoustic (LA) branch appeared in the wide energy region from 0 to 140 meV in the dispersion curves, and the large dispersion of the LA phonon is a characteristic feature of materials with strong chemical bonds. The energies of both the longitudinal optical (LO) and LA phonon bands of the m-BC$_3$ were lower than those of the s-BC$_3$. Especially, the energy of the LO phonon mode [see Fig. 7(a)] was largely reduced by about 20 meV, which is mainly due to the reduction of the in-plane-nearest-neighbor stretching force constants. On the contrary, no large difference in the energies of the ZO, ZO′, and ZA phonons between the two BC$_3$ sheets was found. Compared with the phonon energies of the clean NbB$_2$(0001) surface,[29] all of the observed phonon energies of the two sheets were different except for the ZA branches.
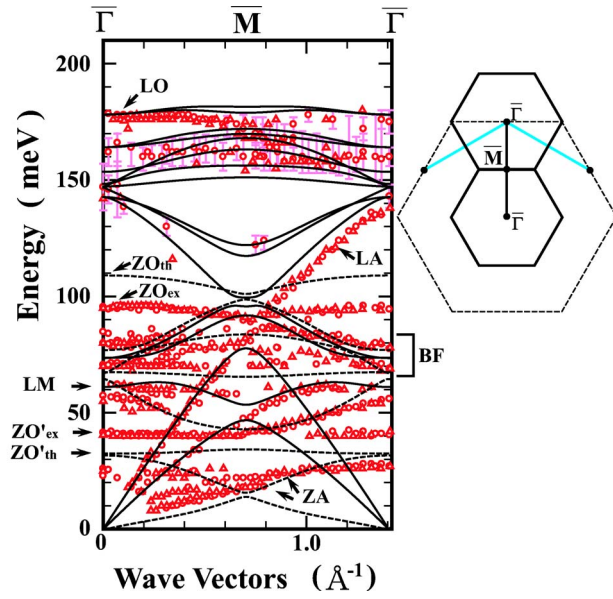
FIG. 5. (Color online) The observed dispersion curves along the $\bar{\Gamma}$-$\bar{M}$ axis of the s-BC$_3$ sheets (red open circles for E_0 of 18.1 eV, red open triangles for E_0 of 24.7 eV), and the theoretical curves obtained based on the *ab initio* calculation (solid lines for phonons with in-plane polarization, broken lines for phonons with out-of-plane polarization). Some characteristic branches are denoted by capital letters. A hexagonal zone framed by dashed lines represents a 1×1 BZ, and hexagonal zones framed by solid lines represent 2×2 BZs (see the text).
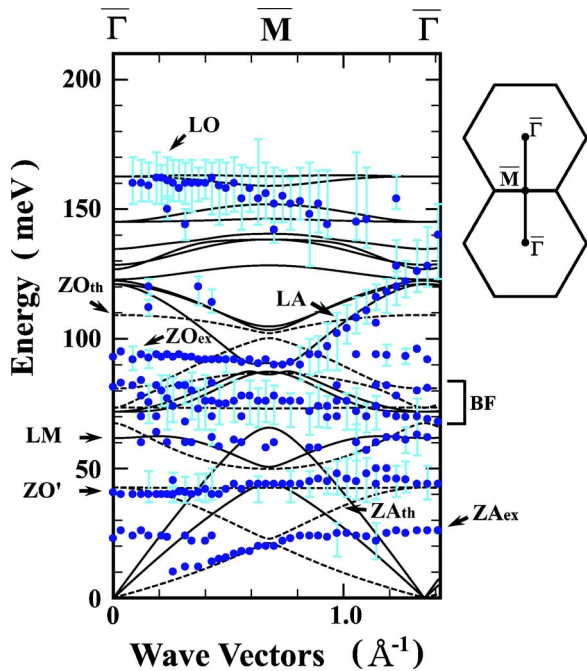
FIG. 6. (Color online) The observed dispersion curves along the $\bar{\Gamma}$-$\bar{M}$ axis of the m-BC$_3$ sheets (blue solid circles for E_0 of 24.7 eV) and the theoretical curves obtained based on the *ab initio* calculation (solid lines for phonons with in-plane polarization, broken lines for phonons with out-of-plane polarization). Some characteristic branches are denoted by capital letters, see the text. Hexagonal zones framed by solid lines represent the SBZs of BC$_3$.
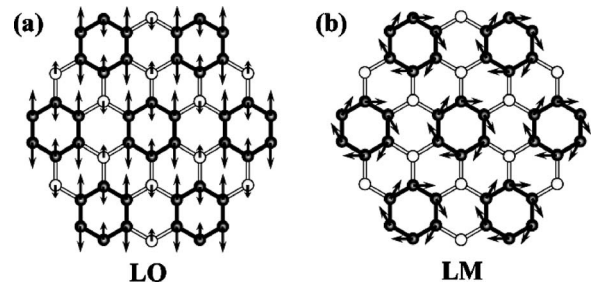
FIG. 7. The atomic displacements of the BC$_3$ sheet associated with the phonons at the $\bar{\Gamma}$ point: (a) the longitudinal optical (LO) phonon and (b) the librational mode (LM) as denoted in Figs. 4–6. Arrows indicate the directions of the atomic displacements from the equilibrium positions.

Figures 5 and 6 show the theoretical curves along the $\bar{\Gamma}$-$\bar{M}$ axis of the s- and m-BC$_3$ sheets, together with the experimental data points in Fig. 4. Solid and broken lines represent phonon branches with in-plane and out-of-plane polarization, respectively. For both the BC$_3$ sheets, most of the experimental curves, particularly the phonons with in-plane polarization, were reproducible on the basis of the *ab initio* calculations of the lattice dynamics, and the exceptional ones were the phonons with out-of-plane polarization as typified by the ZO, ZO′, and ZA. Those vibrational energies disagreed with the experimental ones. The disagreement is attributed to an interaction with the substrate,[30,31] because the monolayer model used in this calculation does not address the interaction.
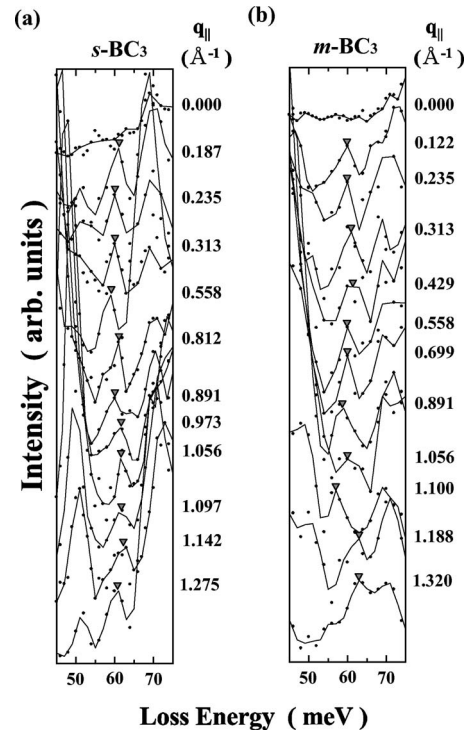
FIG. 8. The HREEL spectra of the s- and m-BC$_3$ sheets ranging from 45 to 75 meV measured by E_0 of 24.7 eV. The energy loss peaks around 60 meV are denoted by triangles.

TABLE I. A list of the stretching force constants (FCs) and their bond lengths of the nearest-neighbor bonds in graphite, the *s*- and *m*-BC$_3$, diamond *h*-BN, *c*-BN, B$_4$C, B$_4$C, NbB$_2$, and ZrB$_2$. The FCs of the C-C and B-C bonds from the first column to the fourth column were calculated based on the *ab initio* calculations. The FCs of the C-C, B-N, and B-B bonds from the fifth column to the last column were determined as the fitting parameters in the force constant model (Refs. 13, 29, 30, and 34–38).

	$F_{C\text{-}C}(l_{C\text{-}C})$ $(10^4$ dyn/cm) (nm)	$F_{B\text{-}C}(l_{B\text{-}C})$ $(10^4$ dyn/cm) (nm)	$F_{B\text{-}N}(l_{B\text{-}N})$ $(10^4$ dyn/cm) (nm)	$F_{B\text{-}B}(l_{B\text{-}B})$ $(10^4$ dyn/cm) (nm)
s-BC$_2$ (this work)	41.2 (0.142)	27.9 (0.156)		
m-BC$_3$ (this work)	30.5 (0.146)	17.0 (0.164)		
Graphite-*ab initio*	41.6[a] (142[a])			
B$_4$C-*ab initio*		57[e] (0.142[e])		
Graphite-fitting	36.4[b] (0.142[b])			
Diamond	14.9[d] (0.154[d])			
MG/TaC(111)	32.8[b] (0.146[b])			
MG/HfC(111)	34.6[b] (0.144[b])			
MG/NbC(111)	33.9[b] (0.145[b])			
MG/TiC(111)	34.6[b] (0.144[b])			
MG/TaC(001)	36.3[b] (0.142[b])			
MG/NbC(001)	39.4[b] (0.143[b])			
MG/WC(0001)	33.6[b] (0.142[b])			
MG/Ni(111)	32.4[b] (0.144[b])			
MG/Pt(111)	39.4[b] (0.142[b])			
h-BN			33.1[f] (0.144[f])	
c-BN			14[g] (0.156[g])	
NbB$_2$				8.8[c] (0.180[c])
ZrB$_2$				7.4[c] (0.183[c])

[a]Reference 13.
[b]Reference 30.
[c]Reference 29.
[d]References 34 and 35.
[e]Reference 36
[f]Reference 37.
[g]Reference 38.

Lastly, we shall discuss some characteristic phonon branches of the BC$_3$ sheets originating from their large unit cell with respect to that of graphite. One is a rotational-like vibration mode of carbon hexagons, which we call the librational mode (LM). The eigenmode at the point is depicted in Fig. 7(b). The theoretical calculation indicated that the LM was observed around 60 meV in each BC$_3$. There were no differences in the energies of the LM between the *s*- and *m*-BC$_3$ sheets both theoretically and experimentally. Figure 8 shows the enlarged phonon spectra of the two BC$_3$ sheets ranging from 45 to 75 meV. Weak peaks around 60 meV were observed in both the spectra. The lack of the peak around 60 meV in the specular spectra at $q_\parallel = 0$ indicates that the phonons have in-plane polarization. The restoring force for the displacement in the LM originates from the B-C bond bending. The theoretical and experimental results indicate that the restoring force of the B-C bond bending is relatively insensitive to the change of the bond length. Concerning the B-B bonds, similar rotational-like modes of boron icosahedron were reported in α-boron;[32] the librational energy of the whole icosahedron around one of the two axes orthogonal to the [111] rhombohedral axis observed in the α-boron was 65 meV, and the other LM, about the [111] axis, appeared at 63 meV. Moreover, the librational energies in the other materials such as the B$_{12}$C$_3$, B$_{12}$P$_2$, and B$_{12}$As$_2$ were 66, 64, and 63 meV,[33] respectively.

The second feature of the large unit cell is the existence of the phonon bands ranging from 70 to 85 meV, which are denoted by BF in Figs. 5 and 6; they originate from a back-folding 1×1 BZ, namly, a 2×2 BZ. Roughly speaking, the size of the unit cell of BC$_3$ is almost the same as that of the 2×2 structure of monolayer graphite (MG). Hence, extra branches appeared in the 2×2 BZ as compared with those in graphite. In the inset in Fig. 5, we showed a hexagonal zone framed by dashed lines representing the 1×1 BZ, and hexagonal zones by solid lines represent the 2×2 BZs. Regarding the calculated phonon modes ranging from 70 to 80 meV, they mainly originate from the blue lines overlapped with the $\bar{\Gamma}$-$\bar{M}$ axis of the 2×2 BZs by the back-folding. The appearance of the phonons ranging from 70 to 85 meV indicates that the unit cell of the overlayer is almost twice that of MG.

B. Force constants of the *s*- and *m*-BC$_3$ sheets

To clarify the feature of the chemical bonds in the BC$_3$ sheets, we calculated the force constants (FCs) of the nearest-neighbor C-C and B-C bonds for the optimized structures which indicated the theoretical dispersion curves in Figs. 5 and 6. Here, $F_{X\text{-}Y}$ are stretching FCs of nearest-neighbor X-Y bonds. X and Y stand for carbon, boron, or nitrogen. Table I shows a list of $F_{X\text{-}Y}$. These results clearly
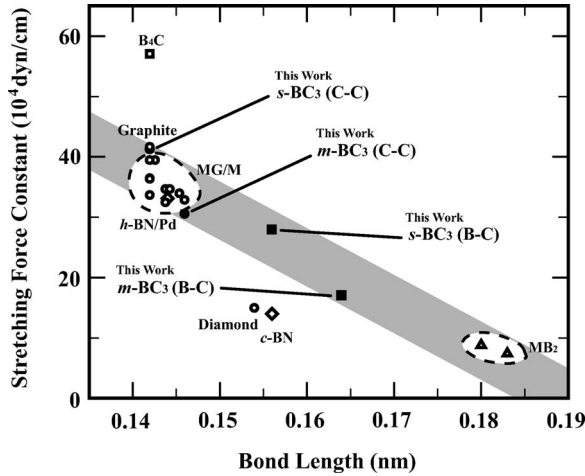
FIG. 9. The stretching force constants versus their bond length of the nearest-neighbor C-C, B-N, B-C, and B-B bonds. The F_{C-C} and F_{B-C} of the s- and m-BC$_3$ sheet are indicated by solid circles and solid squares, respectively. Open circles represent the F_{C-C} of graphite, monolayer graphite grown on metal substrate (MG/M), and diamond crystal. Open diamonds represent the F_{B-N} of h-BN and c-BN. Open squares represent the F_{B-C} of B$_4$C. Open triangles represent the F_{B-B} metal diboride (MB$_2$) such as NbB$_2$, ZrB$_2$. Their values are listed in Table I.

indicate that the stretching FCs are sensitive to the changes in the bond lengths; the F_{C-C} and F_{B-C} of the m-BC$_3$ was about two-thirds of those of the s-BC$_3$, while the l_{C-C} and l_{B-C} of the m-BC$_3$ was about a few percent longer than those of the s-BC$_3$.

In Fig. 9, we plotted these stretching FCs against the bond lengths of various materials, which are the BC$_3$ sheets, graphite,[13,30] monolayer graphites on metal substrate (MG/M),[30] diamond,[34,35] B$_4$C,[36] h-BN,[37] *cubic* boron nitride (c-BN),[38] and metal diborides (MB$_2$).[29] They are listed in Table I. The data points of open circles, open diamonds, open squares, and open triangles represent the F_{C-C}, F_{B-N}, F_{B-C}, and F_{B-B} in previous works, respectively. Solid circles and solid squares represent the F_{C-C} and F_{B-C} obtained in this work, respectively. The data points of the C-C, B-N, B-C, and B-B bonds in the two-dimensional honeycomb sheets are situated on a common gray band. The FCs change as follows: $F_{C-C}, F_{B-N} > F_{B-C} > F_{B-B}$. The FCs are related to the bond lengths; with increasing the bond length, the FC decreases. A similar relation exists for the single, double, and triple bonds of the nearest-neighbor C-C bonds in molecules such as ethane, ethylene, and acetylene.[39] We emphasize that the relations of three elements, boron, carbon, and nitrogen, are expressed by the one straight band in Fig. 9. It should be noticed that the data point of the B-C bond in the one-dimensional C-B-C chain in B$_4$C deviates from the gray band, and the points of the C-C and B-N bonds in the three-dimensional diamond structure such as diamond and c-BN also deviate from the band. The relations clearly characterize three different chemical bonds; the sp, sp^2, and sp^3 hybridized orbital.

Additionally, the F_{C-C}'S of the BC$_3$ sheets were located at the maximum and minimum points of the sp^2 C-C indicated by the gray band. The F_{C-C} of the s-BC$_3$ was about the

same as that of graphite. The binding energies of the C-C bonds of s-BC$_3$ are also the same. On the other hand, the F_{C-C} of the m-BC$_3$ agreed with the smallest one among those of MG/M.

Lastly, we shall discuss the interaction of the overlayer with the substrate. According to the studies of the monolayer graphite grown on various metal substrates,[30] the phonons of the monolayer graphite changed depending on the substrate. On the active substrates, the phonons softened due to an interaction with the substrate, while on the relatively inert substrates, the phonons were same as those of the bulk graphite. In the case of the m-BC$_3$ sheets, all the phonons softened, which indicates that the overlayer interacts with the substrate. On the other hand, in the case of the s-BC$_3$, only the out-of-plane phonons softened, and the in-plane phonons did not; this result means that the C-C bond of the s-BC$_3$ was not largely influenced by the substrate. To discuss the interaction between the substrate and the two BC$_3$ sheets in detail, we have to take into account changes in the structure involving the substrate such as the niobium (Nb) atoms at the second layer. In fact, the LEED spots of the s-BC$_3$ overlayer are much more intensive than those of the substrate for all the electron energy; this suggests strongly that the Nb atoms at second layer are clinging to the s-BC$_3$ sheets in a commensurate manner, and contributed to the LEED intensity. However, so far, we could not obtain any data concerning their detailed position. Theoretical investigations would clarify this point in future work.

IV. SUMMARY

The phonon-dispersion curves of the s- and m-BC$_3$ honeycomb sheets have been investigated experimentally and theoretically. The experimental curves were in good accordance with the *ab initio* calculations. We found a common relationship between the stretching force constants and the bond lengths of the two-dimensional honeycomb sheets constituted by boron, carbon, and nitrogen, which was different from those in the one- and three-dimensional bonding. We characterized the stretching force constants of the nearest-neighbor C-C and B-C bonds in the BC$_3$ sheets quantitatively. In addition, from the observed phonon eneries of the librational mode of carbon hexagons, we also characterized the bending FCs of the nearest-neighbor B-C bonds in the BC$_3$ sheets.

*Electronic address: hyanagisawa@ruri.waseda.jp

[1] H. W. Kroto, J. R. Heath, S. C. O'Brien, and R. E. Smally, Nature (London) **318**, 162 (1985).

[2] S. Iijima, Nature (London) **354**, 56 (1991).

[3] A. Nagashima, N. Tejima, Y. Gamou, T. Kawai, and C. Oshima, Phys. Rev. Lett. **75**, 3918 (1995).

[4] E. Rokuta, Y. Hasegawa, K. Suzuki, Y. Gamou, C. Oshima, and A. Nagashima, Phys. Rev. Lett. **79**, 4609 (1997).

[5] M. J. Mehl, D. A. Papaconstantopoulos, and D. J. Singh, Phys. Rev. B **64**, 140509(R) (2001).

[6] H. Rosner, A. Kitaigorodsky, and W. E. Pickett, Phys. Rev. Lett. **88**, 127001 (2002).

[7] R. A. Jishi, M. Benkraouda, and J. Bragin, Phys. Lett. A **306**, 358 (2003).

[8] F. J. Ribeiro and M. L. Cohen, Phys. Rev. B **69**, 212507 (2004).

[9] J. Nagamatsu, N. Nakagawa, T. Muranaka, Y. Zenitani, and J. Akimitsu, Nature (London) **410**, 63 (2001).

[10] J. Kouvetakis, R. B. Kaner, M. L. Sattler, and N. Bartlett, J. Chem. Soc., Chem. Commun. **1986**, 1758 (1986).

[11] K. M. Krishnan, Appl. Phys. Lett. **58**, 1857 (1991).

[12] H. Tanaka, Y. Kawamata, H. Simizu, T. Fujita, H. Yanagisawa, S. Otani, and C. Oshima, Solid State Commun. **136**, 22 (2005).

[13] H. Yanagisawa, T. Tanaka, Y. Ishida, M. Matsue, E. Rokuta, S. Otani, and C. Oshima, Phys. Rev. Lett. **93**, 177003 (2004).

[14] H. Yanagisawa, Y. Ishida, T. Tanaka, S. Otani, and C. Oshima (unpublished).

[15] S. Otani, M. M. Korsukova, and T. Mitsuhashi, J. Cryst. Growth **194**, 430 (1998).

[16] The software package has been provided by the CAMP project. Accessible URL on internet is http://www.fysik.dtu.dk

[17] D. Vanderbilt, Phys. Rev. B **41**, R7892 (1990).

[18] J. P. Perdew, J. A. Chevary, S. H. Vosko, Koblar A. Jackson, Mark R. Pederson, D. J. Singh, and Carlos Fiolhais, Phys. Rev. B **46**, 6671 (1992).

[19] H. J. Monkhorst and J. D. Pack, Phys. Rev. B **13**, 5188 (1976).

[20] K. Kunc and R. M. Martin, Phys. Rev. Lett. **48**, 406 (1982); K. Kunc and P. G. Dacosta, Phys. Rev. B **32**, 2010 (1985).

[21] O. Dubay and G. Kresse, Phys. Rev. B **67**, 035401 (2004).

[22] H. Yanagisawa, T. Tanaka, Y. Ishida, M. Matsue, E. Rokuta, S. Otani, and C. Oshima, Surf. Interface Anal. **37**, 133 (2005).

[23] Q. Wang, L.-Q. Chen, and J. F. Annett, Phys. Rev. B **54**, R2271 (1996).

[24] D. Tomanek, R. M. Wentzcovitch, S. G. Louie, and M. L. Cohen, Phys. Rev. B **37**, 3134 (1988).

[25] We have found that the B-C bond length of the s-BC_3 in our previous letter[13] was underestimated by 0.001 nm. The difference of bond length, however, did not affect the conclusions in the letter.

[26] C. Oshima, T. Aizawa, R. Souda, Y. Ishizawa, and Y. Sumiyoshi, Solid State Commun. **65**, 1601 (1988).

[27] A. Ueno, T. Fujita, H. Yanagisawa, S. Otani and C. Oshima (unpublished).

[28] K.-P. Bohnen, R. Heid, and B. Renker, Phys. Rev. Lett. **86**, 5771 (2001).

[29] T. Aizawa, W. Hayami, and S. Otani, Phys. Rev. B **65**, 024303 (2001).

[30] T. Aizawa, R. Souda, S. Otani, Y. Ishizawa, and C. Oshima, Phys. Rev. B **42**, 11469 (1990).

[31] A. Nagashima, K. Nuka, H. Itoh, T. Ichinokawa, S. Otani, and C. Oshima, Surf. Sci. **291**, 93 (1993).

[32] N. Vast, S. Baroni, G. Zerah, J. M. Besson, A. Polian, M. Grimsditch, and J. C. Chervin, Phys. Rev. Lett. **78**, 693 (1997).

[33] D. R. Tallant, T. L. Aselage, A. N. Campbell, and D. Emin, Phys. Rev. B **40**, 5649 (1989).

[34] A. D. Zdetsis, Chem. Phys. **40**, 345 (1979).

[35] T. Yamanaka, S. Morimoto, and H. Kanda, Phys. Rev. B **49**, 9341 (1994).

[36] H. Yanagisawa, T. Tanaka, Y. Ishida, S. Otani, and C. Oshima (unpublished).

[37] E. Rokuta, Doctral thesis, Waseda University, 1999.

[38] K. Kim, W. R. L. Lambrecht, and B. Segall, Phys. Rev. B **53**, 16310 (1996).

[39] G. C. Pimentel and R. D. Spratley, *Chemical Bonding Clarified Through Quantum Mechanics* (Holden-Day, San Francisco, 1969).